

## 1. INTRODUCTION AND PRINCIPAL RESULTS<sup>1</sup>

### Shipboard Scientific Party<sup>2</sup>

#### INTRODUCTION

Hydrothermal circulation is one of the fundamental processes associated with crustal accretion along oceanic spreading centers. Driven by heat from magmatic intrusions and emplacement of new crust, seawater circulates through the permeable portions of the crust and the upper mantle (e.g., Lister, 1974; Strens and Cann, 1986) and discharges at the seafloor as both high-temperature (up to 400°C), focused fluid flow and lower temperature (less than ~250°C), diffuse fluid flow. The transport of heat from the lithosphere to the hydrosphere by this process has been estimated to account for about 30% of the predicted global oceanic heat flux, which in turn comprises almost 25% of the total heat flux of the Earth (e.g., Sclater et al., 1980; Stein and Stein, 1994).

Circulating hydrothermal fluids interact with the oceanic basement in a complex series of water-rock reactions that not only influence the physical properties and composition of the crust (e.g., Thompson, 1983; Jacobson, 1992; Johnson and Semyan, 1994), but also give rise to the development of seafloor mineral deposits. These reactions result in changes in the chemistry of the material recycled into the mantle by subduction (e.g., Hoffmann and White, 1982; Hart and Staudigel, 1989) and also play a role in regulating the chemical composition of seawater (e.g., Edmond et al., 1979). However, the extent of alteration and its impact on global geochemical mass balances is still very poorly constrained. Hydrothermal vent systems also provide unique habitats that support chemosynthetically based biological communities that are especially adapted to the physicochemical environment and ephemeral nature of vents.

Submarine hydrothermal systems have now been described from fast, intermediate, and slow spreading ridges; at intraplate volcanic centers; and in island arc settings, both in backarc basins and in forearc regions (a listing of areas of seafloor mineralization and their characteristics has recently been compiled by Rona and Scott, 1993). Despite the diverse range of volcanic and tectonic environments in which hydrothermal systems occur, the fundamental process of thermally driven seawater circulation within the basement is the same. However, detailed sampling of vent fluids and precipitates from submersibles, combined with geophysical data and biological survey information, indicate that considerable differences exist in the size, morphology, and composition of the mineral deposits, in the chemistry of the discharging fluids, and in the makeup of the associated biological communities.

Much of our knowledge of the subsurface part of the hydrothermal system has been derived from studies of altered rocks recovered from oceanic spreading centers (e.g., Bonatti et al., 1976; Humphris and Thompson, 1978; Alt et al., 1986; Mével, 1987; Gillis and Thompson, 1993) and from ophiolites (e.g., Stern and Elthon, 1979; Harper et al., 1988; Nehlig and Juteau, 1988; Gillis and Robinson,

1990). A wide range of alteration assemblages have been described that result from water-rock reactions that progressively change as the physical and chemical conditions within the circulation system evolve. Experimental work has provided thermodynamic data for important mineral phases and aqueous complexes, as well as constraints on the mobilities of elements under different physical and chemical conditions (see review by Saccocia et al., 1994). Theoretical modeling has examined the transfer of heat from a magma chamber to the circulating fluid, as well as the relations between permeability and fluid flow within hydrothermal systems (e.g., Lowell et al., 1993, 1995; Rosenberg et al., 1993). All of these approaches have been combined into simple conceptual models of the progression of alteration reactions that occur within the oceanic crust. These have been summarized in Gillis and Thompson (1993) and Alt (in press), and include initial stages of oxidation at low temperatures (up to 150°C) during recharge of seawater into the crust, with precipitation of anhydrite and reduction of sulfate as the fluid is heated. With increasing temperatures and depth, certain elements are leached from the volcanic section and higher temperature mineral assemblages are formed (e.g., greenschist and amphibolite facies). Penetration of the hydrothermal fluid to greater depths within the dikes and gabbros results in leaching of metals and sulfur from the rocks. As the hot hydrothermal fluids rise, sulfide mineralization occurs both within the upper crust as well as on the seafloor as a result of mixing between seawater and hydrothermal fluids.

Deep-sea hydrothermal vents also provide a unique environment for the study of thermally restricted, hyperthermophilic microorganisms (organisms that grow optimally above 80°C) that are supported by gases such as CO<sub>2</sub>, H<sub>2</sub>, NH<sub>3</sub> and CO in the high-temperature fluids (Baross and Deming, 1995). These primary producers provide the basis of the trophic structure that supports the large biomass of macro-invertebrates endemic to deep-sea hydrothermal vents. The microorganisms may also be present underlying the seafloor vents in a subsurface biosphere (Reysenbach and Deming, 1991; Deming and Baross, 1993); this has important implications for the microbial ecology at the vents and for theories on the origin of life.

Despite all of the studies on oceanic hydrothermal systems, as well as on ancient mineral deposits within a number of ophiolite complexes on land, many uncertainties remain about the nature of the subsurface part of an active system. These include (1) the permeability, pressure, and temperature structure within the upflow zone beneath an active hydrothermal system; (2) the nature of the chemical reactions between water and rock in both the upflow zone and the underlying reaction zone; (3) the mechanisms of sulfide precipitation and subsequent modification below the seafloor; (4) structural controls on the plumbing system within both the upflow and reaction zones; (5) the evolution of major black smoker systems; and (6) the existence, extent, and persistence of a subsurface biosphere.

Ocean Drilling Program (ODP) Leg 158 was designed to address these issues by investigating fluid flow, alteration and mineralization, and associated geochemical fluxes, microbiological processes, and the subsurface nature of an active hydrothermal system on a slow-spreading, sediment-free mid-ocean ridge. Hydrothermal systems on unsedimented mid-ocean ridges dominate global hydrothermal activ-

<sup>1</sup>Humphris, S.E., Herzig, P.M., Miller, D.J., et al., 1996. *Proc. ODP, Init. Repts.*, 158: College Station, TX (Ocean Drilling Program).

<sup>2</sup>Shipboard Scientific Party is as given in the list of participants in the contents.

ity and, hence, are an important contributor to global mass and energy fluxes. The site chosen for this study was the active Trans-Atlantic Geotraverse (TAG) hydrothermal mound (26°08'N on the Mid-Atlantic Ridge), a large, mature deposit composed of massive sulfides estimated to be in excess of 5 million metric tons (Rona et al., 1986), making it equivalent in size to some of the ore deposits on land, such as in the Cyprus, Oman, and other ophiolites (e.g., Constantinou and Govett, 1973; Ixer et al., 1984).

### Geologic Setting of the TAG Segment

The 40-km-long ridge segment in which the TAG hydrothermal field is located (Fig. 1) trends north-northeasterly and is bounded by nontransform discontinuities to the south and north at 25°55'N and 26°17'N, respectively (Purdy et al., 1990; Sempéré et al., 1990). Seafloor spreading has been asymmetric over the last 10 m.y., with half spreading rates of 13 mm/yr to the east and 11 mm/yr to the west (McGregor et al., 1977).

The seafloor morphology of the TAG ridge segment has been well defined by SeaBeam bathymetric surveys of the Mid-Atlantic Ridge (Purdy et al., 1990; Sempéré et al., 1990). The segment has a morphology typical of the 15 to 18 ridge segments lying between the Kane and Atlantis fracture zones (Sempéré et al., 1990; Smith and Cann, 1992). In plan view, the floor of the median valley has an hour-glass shape, narrowing and shallowing toward the center of the segment at about 26°10'N. In cross section, the median valley has an asymmetrical shape, the eastern wall being higher, steeper, and smoother than the western wall (Zonenshain et al., 1989; Karson and Rona, 1990). Using SeaBeam and high-resolution, deep-towed, side-scan sonar data, Smith and Cann (1990, 1993) documented the style of crustal accretion from 24° to 30°N. Along this section of the MAR, the floor of the median valley is built of superposed, small-scale seamounts, with the axial volcanic ridges being formed by overlapping individual volcanic edifices.

Additional data on the geological structure of this segment, primarily concentrated in the vicinity of the hydrothermal field, have been collected from deep-towed camera profiles, piston-coring, water temperature profiling, dredging, submersible dives (Rona, 1980; Rona et al., 1984, 1986; Eberhart et al., 1988; Thompson et al., 1988; Karson and Rona, 1990) and, most recently, from a 120-kHz, side-scan sonar survey with high-resolution, co-registered bathymetry (Kleinrock et al., 1994, this volume). The western wall of the median valley consists of fault-controlled basaltic scarps and sediment-covered terraces (Eberhart et al., 1988; Zonenshain et al., 1989; Kleinrock et al., 1994). Much of the eastern wall is covered with basaltic debris-slide deposits partly buried by calcareous ooze; fault scarps range in height from 10 to 20 m but locally reach heights up to 150 m (Karson and Rona, 1990). Outcrops of pillow lavas were also observed on the eastern wall (Zonenshain et al., 1989). Karson and Rona (1990) suggested that generally east-west-trending scarps exposed in a reentrant in the east wall are part of a transfer fault zone that accommodates differential movement between adjacent normal fault blocks. They stressed the role of intersections of axis-transverse with axis-parallel fault systems in localizing the active sulfide mound by creating permeability pathways that focus high-temperature upflow. In the vicinity of the TAG hydrothermal field, Kleinrock et al. (1994, this volume) have identified a concentrated zone of rift-parallel (north-northeast) fissures and faults that are actively developing and crosscutting a series of preexisting east-northeast-trending faults.

Important constraints on the along-axis changes in stress state and seismic velocity structure are provided by a microearthquake survey and seismic refraction experiment conducted on this ridge segment (Kong, 1990; Kong et al., 1992). These studies suggest that most of the microearthquake activity occurs at the axial high at the center of the segment; earthquakes are also distributed along-axis and in the eastern rift valley walls. No seismic events were detected beneath the

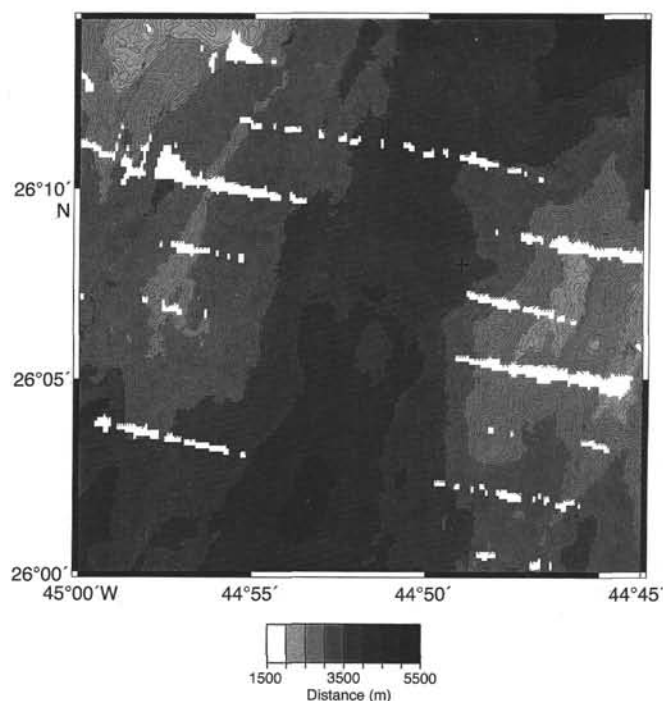


Figure 1. SeaBeam bathymetry of the TAG segment showing the location of the active hydrothermal mound (+). Contour interval is equal to 50 m (from Purdy et al., 1990).

active TAG hydrothermal mound. The maximum depth of seismicity shoals toward the center of the segment, where a low-velocity zone is observed. The distribution of seismicity, the low-velocity zone, and the recent hydrothermal activity suggest recent crustal injection near the axial high. Sea-surface gravity data indicate that the TAG segment contains a "bull's eye" anomaly (Lin et al., 1990), suggesting that either the crust is anomalously thick or that anomalously warm mantle upwells buoyantly beneath this ridge segment.

Magnetic field data from regional surface ship studies indicate that a broad north-northeast-trending area of low residual magnetic intensity about 12 km long and 8 km wide is associated with the TAG hydrothermal field (McGregor and Rona, 1975; Tivey et al., 1989; Wooldridge et al., 1992). This has been interpreted to result from hydrothermal alteration of the basaltic crust (Wooldridge et al., 1992) or by a combination of alteration focused at the hydrothermal zones and broader thermal demagnetization for the TAG hydrothermal field as a whole (Tivey et al., 1993).

### Geology and Tectonic Setting of the TAG Hydrothermal Field

The geologic and tectonic settings of the TAG hydrothermal field have recently been summarized in Rona et al. (1993a). At about 26°10'N (approximately the middle of the segment) the east wall forms a broad salient that reduces the width of the valley floor from about 9 to 6 km and rises from the valley floor, near 4000 m depth, to a height of 2000 m through a series of steps formed by fault blocks (Temple et al., 1979). The TAG hydrothermal field is located at the base of this salient and extends over an area at least 5 × 5 km along the eastern median valley wall (Fig. 2). It consists of presently active low- and high-temperature zones, as well as a number of relict deposits. The zone of low-temperature activity occurs between 2400 and 3100 m depth on the east wall and includes massive, layered deposits

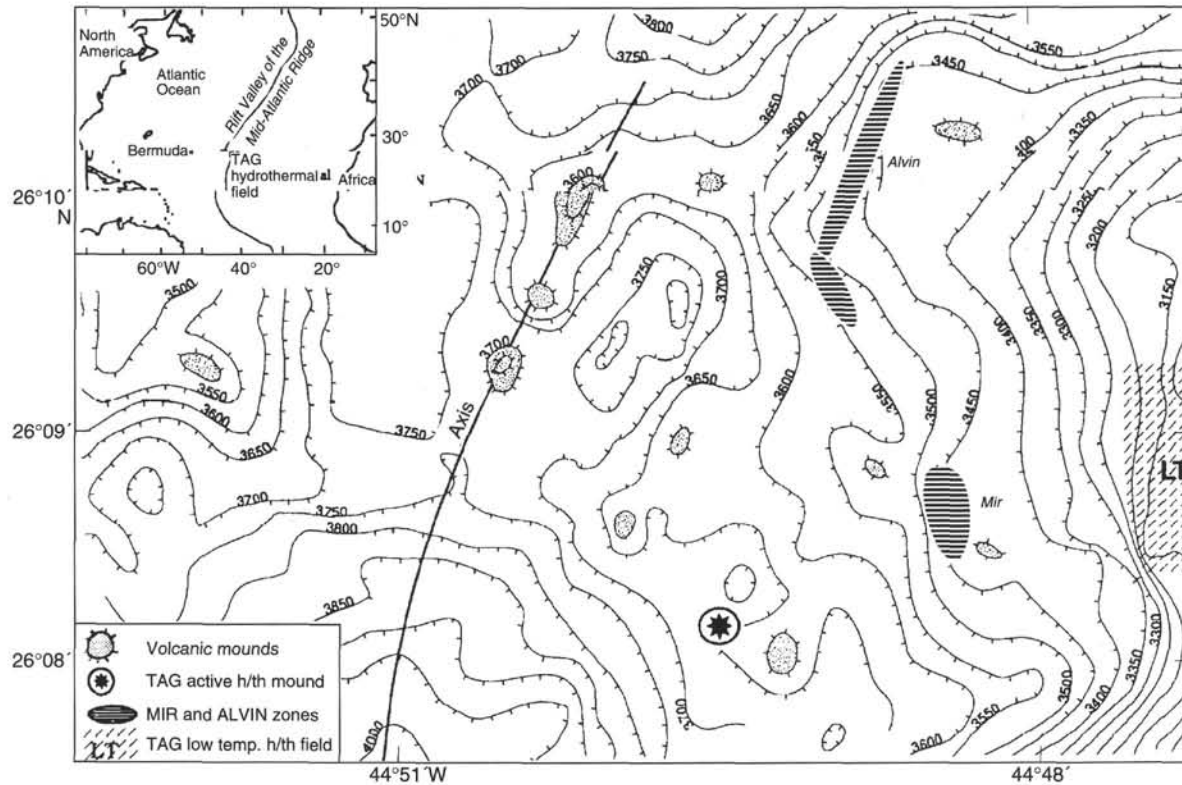


Figure 2. SeaBeam bathymetry (50-m contour interval) of the TAG hydrothermal (h/th) field showing the locations of volcanic domes, the active TAG hydrothermal mound, the low-temperature hydrothermal field up on the eastern rift valley wall, and the *Alvin* and *Mir* relict hydrothermal zones (after Rona et al., 1993b).

of manganese oxide (birnessite), Fe-oxide (amorphous), and Fe-silicate (nontronite) (Rona et al., 1984; Thompson et al., 1985).

Two large relict zones occur on the lower east wall to the north of the active mound; these are thought to be associated with volcanic domes (Rona et al., 1993a, 1993b) (Fig. 2). The 2-km-long *Alvin* hydrothermal zone is located between depths of 3400 and 3600 m and is comprised of discontinuous sulfide deposits associated with several moundlike features with similar dimensions to the active mound, and separated by sediment and pillow basalt flows. These moundlike features were identified from near-bottom, camera tows and side-scan sonar imagery. One of the mounds, located at the southern end of the *Alvin* zone, was mapped and sampled during an *Alvin* dive in 1993 (Rona et al., 1993c). This mound appears to have overall dimensions similar to the active mound and is composed of hard aggregates of recrystallized massive pyrite with minor chalcopyrite and sphalerite, the surfaces of which are coated with Fe-oxyhydroxides (Rona et al., 1993b, 1993c). Radiometric dating of sulfide samples from this relict mound consistently yield ages of about 50,000 yr (Lalou et al., 1993a), and heat flow values are relatively low (0.1–0.3 W/m<sup>2</sup>) (Rona et al., 1993c).

The *Mir* zone is located to the south of the *Alvin* zone; it occurs on the lower east wall about 2 km east-northeast of the active mound between 3430 and 3575 mbsl. It contains inactive deposits in various stages of weathering situated on normal fault blocks. Apart from weathered sulfide debris and metalliferous sediments, some areas contain numerous standing and toppled sulfide chimneys, some up to 25 m in length and up to 3 m in diameter (Rona et al., 1993a). A range of sample types has been collected from this area, including chimney debris similar in mineralogy to both the black and the white smokers on the active mound, massive sulfide blocks, Fe-oxide gossan, and manganese-oxide crusts. Almost all samples show signs of extensive

hydrothermal reworking and replacement (Rona et al., 1993a). Radiometric ages for samples from this area range from 140,000 to 9,400 yr and suggest multiple stages of venting (Lalou et al., 1993a).

The presently active black smoker system occurs at the juncture between the rift valley floor and the east wall at approximately 26°08'N, 44°49'W and at a water depth of about 3620–3700 m. The low-temperature field described above lies 3.7 km upslope to the east; the bathymetric axis of the rift valley is about 1.5–2 km to the west. The active high-temperature mound lies on oceanic crust at least 100,000 yr old based on present seafloor spreading rates. Sediment thickness around the active mound is variable depending on the local morphology. *Alvin* studies show that local basins may have >1 m of ooze, steep slopes are bare, and less steep areas have several tens of centimeters of sediment.

A recent high-resolution bathymetric map confirms that the mound is distinctly circular and that it measures 200 m in diameter and about 50 m in height (Fig. 3). It exhibits two distinct platforms at water depths of about 3650 and 3644 m, which may represent two phases of active growth (Humphris et al., 1994). The mound is surrounded by an apron dominated by carbonate and metalliferous sulfide-oxide sediment that ranges in width up to 100 m. A schematic cross section of the active TAG hydrothermal mound made during the 1990 *Alvin* dive series, and the inferred flow pattern within the mound are shown in Figure 4. The mound is composed of massive sulfides and anhydrite, with distinct sample types being distributed from the central to the outer areas of the mound surface (Rona et al., 1993a; Tivey et al., 1995). A cluster of chalcopyrite-anhydrite-rich black smoker chimneys emitting fluids up to 363°C (referred to herein as the Black Smoker Complex) is located northwest of the center of the mound. This chimney cluster sits on the top of a 10- to 15-m high, 20- to 30-m-diameter cone, the surface of which is covered by

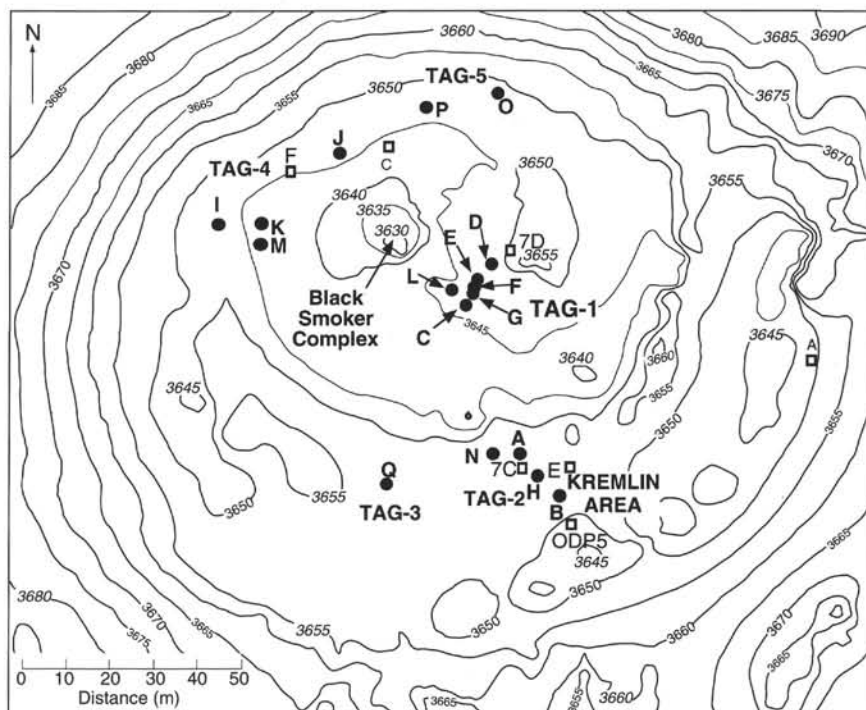


Figure 3. Detailed bathymetry of the active TAG mound derived by phase difference from 120 kHz, side-scan sonar data (see Kleinrock et al., this volume). Locations of the Site 957 drill holes are shown, together with previously emplaced markers that were observed during drilling operations. Open squares = markers, and solid circles = Site 957 holes. Contour interval is 5 m.

a 3- to 6-cm-thick, platelike layer of massive chalcopyrite and marcasite, with interspersed blocks of corroded massive anhydrite with variable amounts of chalcopyrite and pyrite. The tops of both the upper and lower platforms of the mound (at a depth of about 3648 m) are relatively flat with irregular surfaces. Samples of amorphous Fe-oxyhydroxide and silica have been recovered from the west, south, and east rims of the mound; and bulbous, mixed Zn, Fe, and Cu-Fe sulfides with cavities filled by amorphous silica were recovered from the northern rim and central portions of the mound (Tivey et al., 1995). A complex of white smokers venting fluids from 260° to 300°C is located in the southeast quadrant of the mound approximately 70 m away from the Black Smoker Complex; these "Kremlin"-like spires are small (1–2 m) and are composed dominantly of low-Fe sphalerite with minor amounts of chalcopyrite, pyrite, and amorphous silica. Fluids from the white smokers have a very low pH (3 at 23°C) and lesser amounts of iron than the black smoker fluids (Edmond et al., 1995). They are thought to be derived from the black smoker fluids by a combination of conductive cooling and mixing with seawater and precipitation of sulfides within the mound (Edmond et al., 1995; Tivey et al., 1995).

Mass wasting of the edges of the mound results in steep outer slopes to the west, north, and east. Two sample types are exposed: (1) pyrite-rich blocks with trace amounts of late-stage amorphous silica, quartz, and goethite and with outer oxidized layers that include atacamite; and (2) deep-red to orange-brown blocks of amorphous Fe-oxide, goethite, hematite, and silica (as both amorphous silica and quartz). Analogs for these sample types are not found in other known seafloor vent sites, but they are present in the massive sulfide deposits of Cyprus (Herzig et al., 1991).

The distribution of sample types, their mineralogy, and the distinct compositions exhibited at the Black Smoker and Kremlin locations suggest a flow pattern within the mound similar to that shown in Figure 4 (Tivey et al., 1995). Fluids exiting the Black Smoker Complex are extremely focused. Fluids emanating from the Kremlin area have undergone conductive cooling and mixing with seawater, as evidenced by the presence of amorphous silica and by the chemistry of the fluids (Edmond et al., 1995). As the fluid cools and circulates within the mound, pyrite is precipitated. Blocks of this material are exposed during mass wasting.

Preliminary geochronological studies of samples recovered by dredging suggest that the mound is on the order of 40,000 to 50,000 yr old (Lalou et al., 1990). More detailed studies of *Alvin* samples suggest that activity has been intermittent over the past 20,000 yr, with a periodicity of 5000–6000 yr (Lalou et al., 1993b). Present activity began about 50 yr ago after a hiatus of about 5000 yr (Lalou et al., 1993b).

A detailed, near-bottom magnetic survey conducted from *Alvin* in 1990 over the TAG mound showed a magnetization low located directly beneath the mound with a possible dip to the south. This has been interpreted as the alteration pipe of the upflow zone beneath the mound (Tivey et al., 1993).

The convective heat output of the central Black Smoker Complex of the TAG active mound has been calculated to be about 225 MW, based on a set of temperature measurements in the buoyant plume at different altitudes above the vents (Rona et al., 1993b). During the 1993 *Alvin* dive series, about 50 measurements of conductive heat flow were made using 0.6 or 1.0 m probes, which with a few exceptions could be pushed into most locations on and off the mound (Becker et al., 1993; Becker and Von Herzen, this volume). These stations document coherent variations in surface heat flow, which are probably related to subsurface convective patterns. As expected, the highest, and most variable, values were measured in the vicinity of the active Black Smoker Complex. In the Kremlin area described above, conductive heat flow ranges from 3 to 9 W/m<sup>2</sup>. High values (5–10 W/m<sup>2</sup>) were also observed on the southeast edge of the mound, where unfocused, warm (<100°C) water percolates out of the deposits. There is a coherent belt of very low heat flow (<20 mW/m<sup>2</sup>) about 30–40 m west of the black smokers on the flat plateau that surrounds the black smoker cone (Becker and Von Herzen, this volume). This may be an indication of seawater entrainment at this location on the mound.

### Biological Activity on the Active TAG Mound

Hydrothermal activity on the active TAG mound supports a productive chemosynthetic-based benthic community (Van Dover et al., 1988). The most abundant organisms over much of the mound sur-

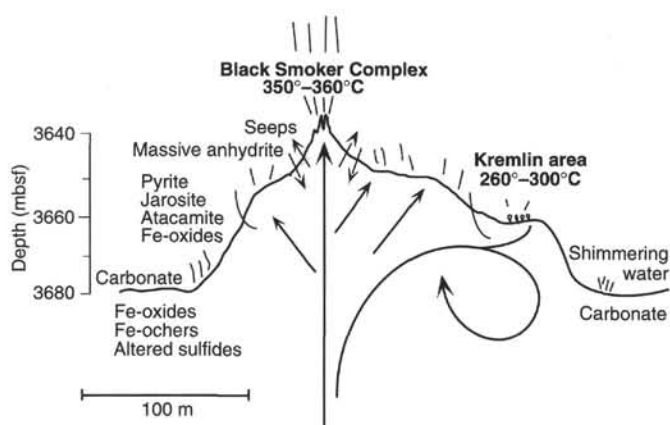


Figure 4. Schematic cross section of the active TAG mound from northwest to southeast. The flow patterns within the mound are derived from the mineralogy and chemistry of the deposits and the chemistry of white smoker and black smoker fluids (from Tivey et al., 1995.)

face where diffuse fluid flow is present are anemones, together with smaller numbers of inconspicuous, tube-dwelling polychaetes and buccinid snails (Grassle et al., 1986; Galkin and Moskalev, 1990). In the immediate vicinity of the active black smokers, however, swarming shrimp (*Rimicaris exoculata*; Rona et al., 1986) that reach densities up to 1500 per square meter are dominant (Van Dover et al., 1988), with two other shrimp species, a brachyuran crab, and a zoarcid fish (at densities of only a few per square meter) also present.

Early evidence suggested that the swarming shrimp mine the surface of sulfide chimneys on which they swarm, digesting the abundant free-living microorganisms that grow there (Wirsen et al., 1993) and egesting the sulfides (Van Dover et al., 1988). It appears that the shrimp lack endosymbionts (Van Dover et al., 1988; Wirsen et al., 1993), contrary to the hypothesis formulated by Gal'chenko et al. (1989). Although conspicuous endosymbiotic invertebrate populations appear to be absent at TAG, the chemosynthetic microbial activity is very productive and diverse. Chemical energy is converted to microbial biomass by lithoautotrophic oxidation of  $H_2S$  and pyrites. The chemoautotrophs are associated with the warm-water emissions, bacterial mats, and the carapaces of the shrimp (Wirsen et al., 1993).

## PRINCIPAL RESULTS

### Introduction

During Leg 158, the subsurface nature of an active, volcanic-hosted hydrothermal system on a slow-spreading ridge was investigated at the TAG hydrothermal mound on the Mid-Atlantic Ridge at approximately 26°N. Drilling was concentrated on a single feature about 200 m in diameter. Consequently, all drilling locations were considered as one site (Site 957), although holes were grouped in specific areas, each of which had distinctive objectives. Several holes in one location were often attempted so that as much of the stratigraphic section as possible could be recovered. It was originally planned that a full logging program would be run at each location and a CORK would be emplaced in one hole; however, because of the extremely difficult drilling conditions, which included hole instability and cleaning problems, we were unable to accomplish these particular objectives. A northwest-southeast transect of three major, distinct areas of the mound was successfully completed, as well as some additional holes to delineate the lateral heterogeneity of the sulfide deposit and the extent and nature of the underlying stockwork zone.

### Site 957

Seventeen holes were drilled at five locations on the active TAG hydrothermal mound (Fig. 3). Six holes were drilled (of which four

produced core) just to the east of the Black Smoker Complex (TAG-1 area) on the upper terrace, and produced a section down to 125 mbsf through the hydrothermal mound and into the upper part of the stockwork zone. Four holes were drilled in the Kremlin area (TAG-2 area) on the lower terrace, where white smokers vent fluids with a chemistry distinct from the black smoker fluids; these holes resulted in maximum penetration of 54.3 mbsf. A single hole was drilled at a second location (TAG-3 area) on the lower terrace south of the Black Smoker Complex and west of the TAG-2 area, but mostly drill cuttings were retrieved down to 14.5 mbsf. Four holes were drilled on the upper terrace on the western side of the mound (TAG-4) to recover a section through the sulfides and into the stockwork zone in an area of low conductive heat flow, and to determine the extent of the sulfides and stockwork in this area. Core was recovered down to 51.2 mbsf. Finally, two holes were drilled on the northeastern side of the upper terrace (TAG-5 area) to determine the lateral heterogeneity of the sulfide mineralization and to delineate the northern extent of the underlying stockwork zone. Coring here penetrated to 59.4 mbsf. In this section, we briefly summarize the stratigraphy at each of the drilling locations.

### TAG-1 Area (East Side of the Black Smoker Complex)

The upper few meters of the core contain fragments of massive granular pyrite and chalcopyrite, which likely represent near-surface hydrothermal precipitates derived from sulfide crusts and chimney talus. From the surface down to 15 mbsf, the core consists dominantly of porous to granular pyrite and pyrite breccias. Below 15 mbsf, an anhydrite-rich zone is present that consists of pyrite-anhydrite and pyrite-silica-anhydrite breccias that extend down to 45 mbsf.

Abundant quartz-pyrite mineralization and quartz veining immediately beneath the anhydrite-rich zone represent the top of the stockwork zone, suggesting that the thickness of the mound in this area is about 30 m. A quartz-rich zone composed mainly of pyrite-silica breccias near the top and silicified wallrock breccias below occurs between about 45 and 100 mbsf. Below about 100 mbsf, the quartz-rich zone grades into a chloritic stockwork where chloritized and weakly mineralized basalt is the dominant lithology. The rocks range from gray chloritized basalt breccias to green chloritized basalt fragments cemented by quartz.

Anhydrite veining is abundant throughout the vertical extent of the section, but it is best developed in the pyrite-anhydrite and pyrite-silica breccias (15–45 mbsf), where veins up to 45 cm in width are present. These veins comprise complex, multistage fracture fillings and cavity linings, some of which include disseminated, fine-grained pyrite and chalcopyrite, and trace amounts of hematite. The occurrence and size of veins decrease downward and correspond to an increase in the amount of quartz.

Large ranges in the chemical compositions of different rock types reflect the extreme heterogeneity of the samples and the variable proportions of sulfides, anhydrite, and silica. The Fe contents of the samples range from 20.1 to 40.8 wt% and reflect the dominance of pyrite in the sulfide section. Copper contents are significantly lower, ranging from 0.01 to 6.0 wt%, and Zn concentrations are also low (<0.12 wt%). The most striking chemical feature of the sulfides in the TAG-1 area is their very low concentrations of Ag, Cd, and Au, all of which are close to their detection limits by AAS.

### TAG-2 Area (“Kremlin” White Smoker)

Hydrothermal precipitates recovered from the topmost section at the TAG-2 Kremlin area include red-brown, sulfide-rich sand and mud (most likely drill cuttings) with abundant chert clasts and a few small pieces of sphalerite and pyrite containing up to 3 wt% Zn and 13 wt% Cu. A hard layer in the top few meters of each hole at TAG-2 consists of mixed pyrite and chert clasts in a dominantly cherty

matrix. Clasts of similar red and gray chert are also common in the underlying massive, porous pyrite to a depth of about 10 mbsf. Most of the sulfide material recovered from the TAG-2 area occurs in the upper 20 m of the section as massive porous pyrite and porous, nodular pyrite breccias in a sandy pyrite matrix. Although the breccias are dominantly matrix-supported, they contain only minor anhydrite cement. The TAG-2 area does not contain as wide a variety of breccias as at the TAG-1 or TAG-4 sites, suggesting that the TAG-2 area has experienced a different history of brecciation, cementation, and veining than similar rocks drilled in the other areas of the mound.

Between 20 and 30 mbsf, the massive pyrite breccias grade into pyrite-silica breccias with anhydrite veining. Silicified wallrock fragments and hyaloclastite first occur at about 30 mbsf, and the wallrock fragments become increasingly abundant with depth. Deeper in the section, the fragments in the pyrite-silica breccias become coarser and more angular and are interspersed with sections of brecciated and silicified wallrock. At about 40 mbsf, the pyrite-silica breccias grade into more massive, silicified wallrock breccias, and chloritized basalt fragments are present locally. These breccias appear to represent the upper part of the stockwork zone.

At the southeastern edge of the TAG-2 area, a section of chloritized pillow-rim breccia with a matrix of chlorite, quartz, and hematite was recovered at the base of the massive sulfides, which overlies partly altered basalt. This is interpreted to be the uppermost basement or a portion of a basaltic flow. The presence of chloritized pillow-rim breccia at the contact between relatively fresh basalt and the base of the massive sulfides indicates less pervasive hydrothermal flow along the margins of the mound.

#### **TAG-3 Area**

##### **(South Side of the Black Smoker Complex)**

Fine- to medium-grained drill cuttings consisting of silt- and sand-sized grains and fragments of massive pyrite, red and gray chert, partially silicified Fe-oxides, and trace amounts of chalcocopyrite were recovered. Geochemical analyses of this material indicate that it is composed of 36.8 wt% S and 33.0 wt% Fe. It has a high Cu content (6.6 wt%) but low concentrations of Zn (0.42 wt%), Ag (5.1 ppm), and Cd (9.2 ppm). These drill cuttings are more pyrite-rich than those recovered in the TAG-2 Kremlin area, and they contain abundant Fe-oxides and chert. They are depleted in anhydrite compared to the drill cuttings on the upper terrace to the north of the Black Smoker Complex (see TAG-5 Area).

#### **TAG-4 Area**

##### **(West Side of the Black Smoker Complex)**

Core recovered from four holes in the TAG-4 area indicates that this part of the mound consists mainly of massive sulfide crusts and sulfide-cemented breccias. In addition, significantly higher amounts of sphalerite, marcasite, and amorphous silica are present in these samples than in samples drilled elsewhere on the mound. Anhydrite is virtually absent in the TAG-4 cores.

In this area, the upper 10 m of the mound consist of porous colloform pyrite + marcasite with red and gray chert and minor chalcocopyrite, below which there is a 10-m-thick zone of massive pyrite and massive pyrite breccia with minor sphalerite and a few altered basalt clasts. Between 20 and 30 mbsf, massive pyrite grades downward into pyrite-silica breccia with abundant silicified wallrock fragments up to 10 cm in size. Silicified wallrock breccias are the dominant lithology between 30 and 42 mbsf, followed by an abrupt transition into slightly to moderately altered basalt having chloritized halos down to 51.2 mbsf.

Geochemical analyses indicate high Fe (38.4–45.7 wt%) and S (41.0–50.8 wt%) contents; Zn concentrations range from 3.0 to 3.7 wt%. The Zn contents are among the highest values determined, whereas Cu contents are only 0.05–0.13 wt%.

Silicified wallrock breccias recovered from the TAG-4 area resemble those in the upper part of the quartz-rich stockwork in the TAG-1 and TAG-2 areas, but they are generally less silicified and contain greater quantities of massive pyrite. The breccias consist of angular to subrounded clasts of variably silicified and highly altered basalt enclosed in a matrix of pyrite-silica breccia or porous massive pyrite. A few pieces of chloritized basalt were recovered below the silicified wallrock breccias. The silicified wallrock and chloritized basalt breccias are underlain by slightly to moderately altered basalts which exhibit chloritized alteration halos and contain veins of quartz, chlorite, and pyrite. X-ray fluorescence analyses of one sample indicate that it is virtually identical to the basalt analyzed from Hole 957B; it has an Mg# of 60.8 and contains 1.67 wt% TiO<sub>2</sub> and 2.42 wt% Na<sub>2</sub>O.

Although abundant wallrock clasts were recovered, the framework-supported nature of the breccias, the absence of pervasive quartz and anhydrite cement, and the presence of only slightly to moderately altered basaltic basement suggest that this area is not part of the high-temperature stockwork. Instead, these breccias appear to be part of a talus pile adjacent to the main upflow zone that, measured from the basalt basement, is at least 20 m thick and is capped by a 10- to 15-m-thick carapace of massive pyrite.

#### **TAG-5 Area**

##### **(North Side of the Black Smoker Complex)**

The overall hydrothermal stratigraphy of the north side of the TAG-5 area is similar to that observed in the TAG-1 area to the east of the Black Smoker Complex. The upper part of the section is comprised dominantly of nodular pyrite and pyrite-anhydrite breccias with minor chalcocopyrite, similar to those in the anhydrite-rich zone in the TAG-1 area. The hard, cherty material encountered in the upper few meters in the TAG-2, TAG-3, and TAG-4 areas was not recovered at TAG-5.

Below 30 mbsf, massive, coarse-grained granular pyrite is associated with the pyrite-silica breccias and contains significant amounts of silica. Remnant patches of chert, dark gray silica, and silicified altered basalt material are commonly included with the massive pyrite, suggesting that the rock formed by pyritization of an existing pyrite-silica or a silicified wallrock breccia. These breccias contain clasts of an earlier generation of pale-gray, fine-grained pyrite-silica breccia, indicating that there have been at least two stages of brecciation. Silicified wallrock breccias and basalt fragments in the lower 25 m are similar to stockwork samples from elsewhere beneath the mound, but they contain greater amounts of pyritic cement.

### **Physical Properties**

Physical properties measurements were made on samples representative of the various rock types sampled from the TAG hydrothermal mound. All of the sulfide-rich rock types have densities that range from 3.2 to 4.7 g/cm<sup>3</sup>, whereas the anhydrite-rich rocks have densities as low as 2.6 g/cm<sup>3</sup>. Most of the rocks sampled had porosities on the order of 2.5%–10%, except for porous sulfides, which contain as much as 30% pore space. Compressional wave velocities ( $V_p$ ) in all sulfide-bearing rocks range from 4.9 to 5.4 km/s, and the moderately altered basalts sampled from the TAG-4 area had an average  $V_p$  of 6.1 km/s. Electrical resistivities measured in various sulfide types were ubiquitously low (<0.6 Ωm), whereas resistivities in anhydrite-rich rocks were significantly higher (as high as 2.8 Ωm). All sulfide-bearing rocks analyzed exhibited high thermal conductivities, ranging from 5.7 to 10.4 W/(m·K).

Paleomagnetic measurements were also made on samples representative of the rock types sampled from different parts of the mound. In general, all sulfide-bearing rocks exhibit a strong, vertically oriented, drilling-induced magnetization, but a relatively low natural remanent intensity. Although alternating-frequency demagnetization

techniques met with varying degrees of success in removing this magnetic overprint, a stable component of magnetism consistent with the location of the TAG mound was isolated with thermal demagnetization techniques. Unblocking temperatures and coercivity determinations indicate that magnetite is the likely magnetic carrier. The results also indicate that magnetic intensity increases with depth in the mound, which suggests that a stratigraphically distinct change in magnetic minerals may exist. The basalts sampled in the TAG-4 area exhibit a natural remanent magnetic character much stronger than normal oceanic basalts, and the isolated stable component of magnetism has a significantly different inclination than expected for the location of the TAG mound ( $14^\circ$  vs.  $55^\circ$ ), which suggests a post-emplacement overprint.

## DISCUSSION

Figure 5 summarizes the inferred stratigraphy for the holes drilled in the three areas that form the northwest-southeast transect of the mound. Because the holes drilled in each area were all in close proximity (typically 10–15 m from each other), their stratigraphy has been considered together to form a composite section at each location.

The most noticeable feature of these sections is the dominance of breccias of various types, not only within the sulfide mound but also extending into the upper part of the stockwork. Comparison of the stratigraphy for each location indicates that, within the mound, pyrite breccias dominate the lithology. Different rock types—massive pyrite breccia, pyrite-anhydrite breccia, and pyrite-silica-anhydrite breccia—are distinguished primarily on the basis of the relative abundances of pyrite, anhydrite, and silica; and they reflect different degrees of brecciation, cementation, hydrothermal reworking, and replacement of preexisting sulfides.

Based on the sequence of rock types recovered from each area, an overall hydrothermal stratigraphy can be developed for the mound and the upper portion of the stockwork. Four major zones can be distinguished, all of which may or may not be present in one section. Clast-supported massive pyrite and pyrite breccias dominate the upper 10–20 m of the mound at every location. This is followed by an anhydrite-rich zone that comprises matrix-supported, pyrite-anhydrite breccias and pyrite-anhydrite-silica breccias in the TAG-1 area. The TAG-5 area, however, contains only vein-related, pyrite-anhydrite breccias. In the TAG-2 area, anhydrite is present only as thin veins and filling vugs; in the TAG-4 area, anhydrite is virtually absent. However, recovery at the TAG-2 and TAG-4 areas was low so that the possibility exists that anhydrite was preferentially not recovered. With increasing depth, the amount of quartz-pyrite mineralization and quartz veining increases and represents the top of the quartz-sulfide stockwork zone, which typically includes pyrite-silica breccias overlying silicified wallrock breccias. This zone was observed at all holes that penetrated >40 mbsf, suggesting that the thickness of the mound is comparable to its relief on the seafloor (Fig. 5). A quartz-chlorite stockwork zone was sampled at depths greater than 100 mbsf in Hole 957E (TAG-1).

The complex assemblage of rock types that result in the overall stratigraphy of the sulfide mound is a product of its multistage development, and is reflected in the sequences of alteration and veining events that can be distinguished both in the sulfide breccias and in the silicified wallrock and chloritized basalt breccias. Sulfide breccias that are now at the base of the mound were formed at the seafloor during an earlier stage of deposit growth and have since been buried and overprinted by later hydrothermal events. The sulfide breccias likely accumulated at the seafloor through the collapse of sulfide structures formed at the seafloor, including large sulfide chimneys and sulfide crusts, and by the dissection of massive sulfides along active fault scarps. This debris has been overgrown by later generations of chim-

neys and progressively cemented or replaced by quartz, sulfides, and sulfates. The presence of altered basalt clasts from the base of the mound higher up in the section may indicate periodic dislocation and partial erosion of the mound/stockwork complex by faults during the growth of the deposit. Alternatively, the basalt clasts may be remnants of lava flows that partially buried the deposit early in its development or relics of the original pillow talus, on top of which the sulfides accumulated.

Variations in the material recovered from the upper few meters at each site provide insights into the formation of new deposits. Fragments of massive granular pyrite and chalcopyrite were recovered in the top few meters at TAG-1; they may represent near-surface hydrothermal precipitates derived from sulfide crusts and chimney talus. Drill cuttings from the top of the section at TAG-2 consisted of sulfide-rich drill cuttings with small pieces of porous massive sphalerite and pyrite. The high Cu and Zn contents (8–13 and 1–3 wt%, respectively) of the sulfide-rich sand suggest that this material may represent near-surface hydrothermal precipitates similar to those recovered at TAG-1. At TAG-4, the massive sulfides that comprise the upper few meters of the section consist of colloform-banded, pyrite-marcasite crusts that exhibit primary depositional textures and high porosity. These sulfides have high Zn contents (3.0–3.7 wt%), and they may be an *in situ* hydrothermal precipitate.

Base metal values are very low within the mound and stockwork zone below the near surface material. However, high Cu values sporadically occur on the selvages of anhydrite veins within the anhydrite-rich zone. The enrichment of base metals in the near-surface part of the mound may be explained by continuous upflow of hydrothermal fluids through predeposited sulfides. The chemical composition and physico-chemical conditions of these fluids cause remobilization of base and precious metals at depth and redeposition of metals caused by the mixing of hydrothermal fluids with ambient seawater near the surface. Similar metal-enriched zones have been observed close to the paleo-sulfide-seawater interface in volcanogenic massive sulfide deposits on land (e.g., Franklin et al., 1981).

Drill cuttings were also recovered from the top of TAG-3, but they were enriched in Fe-oxides and oxyhydroxides. This may reflect oxidation of previously deposited sulfides at this location, but a component of direct hydrothermal precipitation of Fe-oxides may also be present. Similarly, drill cuttings from the top of TAG-4 contain abundant Fe-oxides and are distinctly Cu and Zn poor, closely resembling those collected at TAG-3.

A very hard layer containing red and gray chert was encountered in the upper few meters of the cores recovered from the TAG-2, TAG-3, and TAG-4 areas. This most likely results from the precipitation of silica from hydrothermal fluids percolating through the mound and forming a silica cap. This may be analogous to the silica caps overlying many volcanogenic massive sulfides of land (Franklin et al., 1981).

One of the most remarkable features of the lithology of the mound is the abundance of anhydrite, either as thick veins showing several generations of formation (and dissolution) or as breccia matrix cementing sulfide clasts of various types. Large blocks of anhydrite have also been found during submersible operations at the seafloor near the Black Smoker Complex, which itself is composed dominantly of massive anhydrite. Because of its retrograde solubility at high seafloor pressures and temperatures of <150°C, anhydrite is unstable and dissolves when exposed to seawater. The abundance of anhydrite within the mound indicates that either ambient fluid temperatures are above the solubility limit of anhydrite, or that the anhydrite is isolated from continued exposure to circulating fluids of <150°C. As anhydrite appears to predominate in the major upflow zone beneath the Black Smoker Complex, its abundance is most likely related to the hydrologic regime in this area. The Black Smoker Complex has been estimated to produce heat flow energy in excess of 200 MW (Rona et al., 1993b). This enormous high-velocity discharge of hot fluid forces

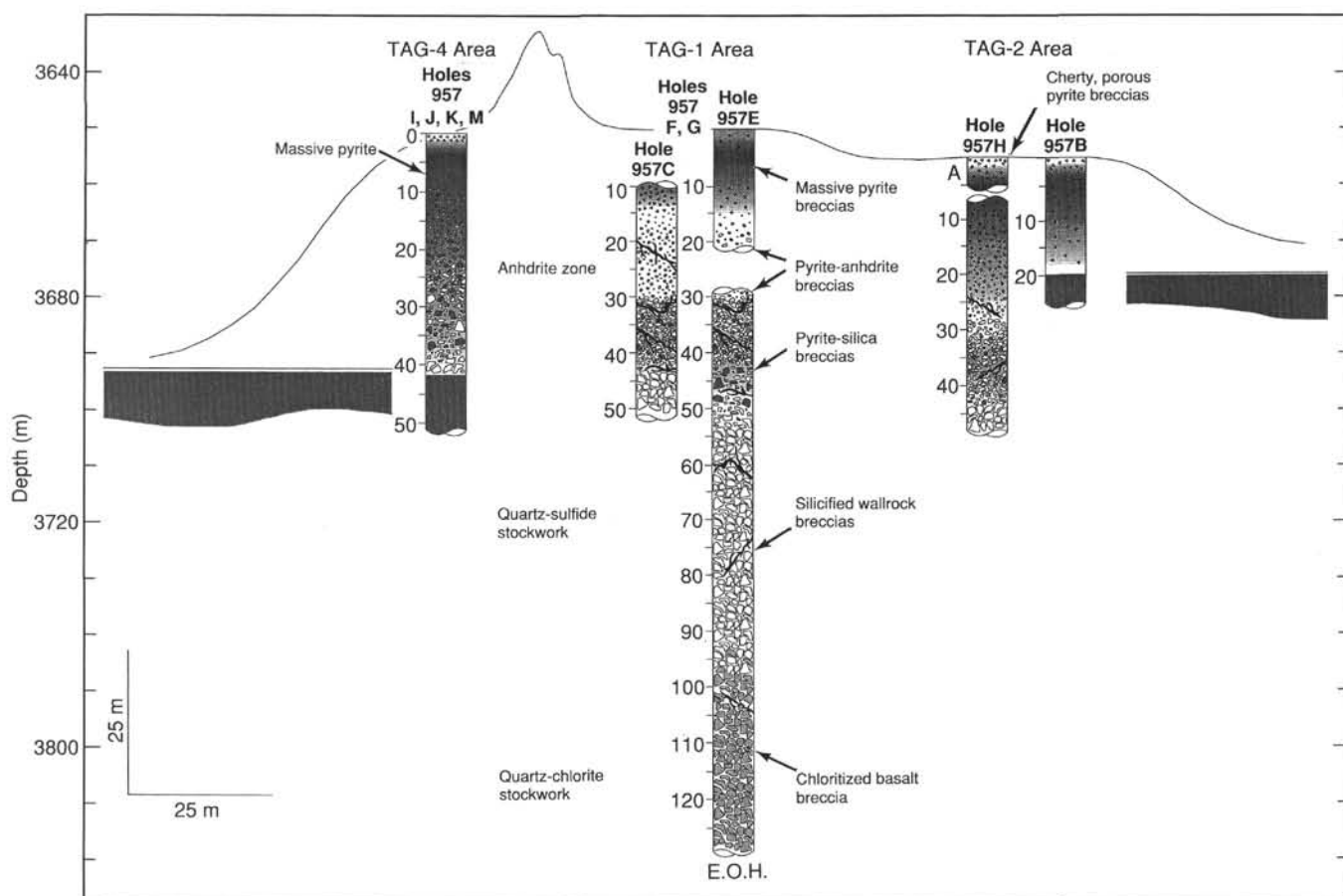


Figure 5. Schematic lithologic stratigraphy of the TAG hydrothermal mound from rocks recovered from the northwest-southeast transect of the TAG-1, TAG-2, and TAG-4 areas. E.O.H. = end of hole.

a major flow of seawater from the edges of the mound into the subsurface of the active Black Smoker Complex. Heating this seawater to temperatures above 150°C by mixing with high-temperature fluid (>360°C) may account for the abundance of anhydrite beneath the central Black Smoker Complex.

Many of the textural and mineralogical characteristics of the TAG mound have implications for Cyprus-type massive sulfide deposits, which are regarded as the closest ancient analogs of massive sulfides currently forming at the mid-ocean ridges. For example, the massive cupriferous sulfides in Cyprus are commonly characterized by the occurrence of "conglomerate ore," which was interpreted to be a product of seafloor weathering and alteration (Constantinou and Govett, 1973). The presence of abundant anhydrite in the subsurface of the TAG mound, however, may indicate that the conglomerate ore of Cyprus was previously deposited as a pyrite-anhydrite breccia and now represents the clasts of this material remaining after the dissolution of the anhydrite cement.

Results from drilling have enabled some constraints to be placed on the vertical and lateral variations in the stockwork beneath the TAG mound. Although the vertical extent of the stockwork zone beneath the TAG-2 area could not be determined, a zonation from silicified to chloritized basaltic clasts occurs about 100 m beneath the top of the deposit. On the western part of the mound (TAG-4), the outer margin of the stockwork zone may be somewhere between the outer edge of the upper terrace and the Black Smoker Complex, and within about 5–10 m of the present high-temperature upflow. Despite their proximity to the present Black Smoker Complex, breccias in this area exhibit only minor veining by anhydrite. The presence of abundant colloform pyrite and late-stage sphalerite in cavities and veins within the mound suggest that low-temperature upflow, possibly originating

from beneath the present Black Smoker Complex, has occurred through the flanks of mound and was likely responsible for cementing the breccias in this area. The low Cu contents of the sulfides are also consistent with little or no high-temperature venting through the talus pile at the edge of the mound.

Basement in the TAG-4 area exhibits heterogeneous alteration, indicating that hydrothermal flow is not pervasive beneath the margins of the mound. Silicified basalt clasts in the wallrock breccias in the TAG-4 area are more consistently rounded than similar clasts elsewhere in the mound.

The recovery of massive pyrite and only slightly to moderately altered basalt in the same section at the base of the mound in the TAG-4 area suggests that there is a sharp contact between hydrothermally altered and mineralized material and the underlying basement. Large clasts of silicified wallrock appear to sit directly on top of unaltered basalt, suggesting that the alteration of the breccias occurred before their emplacement. This altered talus may have been derived from preexisting altered and mineralized pillows beneath the present mound or could have been eroded from an exposed part of the stockwork during an earlier stage in its development. The current position of the high-temperature upflow zone, near the edge of this talus slope, suggests that the Black Smoker Complex may have developed either at the margins of a brecciated massive flow or at the top of a partially eroded fault scarp. The presence of mineralized clasts with different degrees of alteration in the same section (e.g., chloritized fragments together with quartz-rich, mineralized clasts) is consistent with derivation of the talus breccias from a faulted portion of the stockwork.

The observed distribution of intensively reworked silicified wallrock breccias and chloritized basalt breccias at the base of the massive sulfides reveals important information on the formation of the

TAG mound and its strikingly circular shape. A possible scenario may include several stages of evolution and growth of the mound, beginning with volcanic activity and the formation of a volcanic center within the neovolcanic zone. Subsequent spreading-related tectonic activity within the rift valley accounts for the intensive tectonic brecciation of volcanic rocks that results from faulting and the development of a talus pile. Reactivation of these faults at a later stage creates conduits suitable for the upflow of hydrothermal fluids, causing precipitation of massive sulfides and cementation of basalt fragments. The complex sulfide stratigraphy in the TAG mound is a result of repeated episodes of brecciation, cementation, hydrothermal reworking, and sulfide precipitation.

Estimates of tonnage and size of the TAG mound based on the thickness of the sulfide zone and the extent of the underlying stockwork as determined by drilling indicate about 2.7 million metric tons of massive sulfides above the seafloor and approximately 1.2 million metric tons of sulfides in the subseafloor stockwork zone. This amounts to a total of about 4 million metric tons, which is well within the size range for typical ophiolite-hosted massive sulfide deposits worldwide.

## REFERENCES

- Alt, J.C., in press. Subseafloor processes in mid-ocean ridge hydrothermal systems. In Humphris, S.E., Zierenberg, R., Mullineaux, L., and Thompson, R. (Eds.), *Seafloor Hydrothermal Systems: Physical, Chemical, Biological and Geological Interactions within Hydrothermal Systems*. Geophys. Monogr., Am. Geophys. Union.
- Alt, J.C., Honnorez, J., Laverne, C., and Emmermann, R. 1986. Hydrothermal alteration of a 1 km section through the upper oceanic crust, Deep Sea Drilling Project Hole 504B: mineralogy, chemistry, and evolution of seawater-basalt interactions. *J. Geophys. Res.*, 91:10309–10335.
- Baross, J.A., and Deming, J.W., 1995. Growth at high temperatures: isolation and taxonomy, physiology, and ecology. In Karl, D.M. (Ed.), *The Microbiology of Deep-sea Hydrothermal Vent Environments*: Boca Raton, FL (CRC Press).
- Becker, K., Von Herzen, R.P., and Rona, P.A., 1993. Conductive heat flow measurements using *Alvin* at the TAG hydrothermal mound. *Eos*, 74:99.
- Bonatti, E., Honnorez-Guerstein, B.M., and Honnorez, J., 1976. Copper iron sulfide mineralizations from the Equatorial Mid-Atlantic Ridge. *Econ. Geol.*, 71:1515–1525.
- Constantinou, G., and Govett, G.J.S., 1973. Geology, geochemistry, and genesis of Cyprus sulfide deposits. *Econ. Geol.*, 68:843–858.
- Deming, J.W., and Baross, J.A., 1993. Deep-sea smokers: windows to a subsurface biosphere. *Geochim. Cosmochim. Acta*, 57:3219–3230.
- Eberhart, G.L., Rona, P.A., and Honnorez, J., 1988. Geologic controls of hydrothermal activity in the Mid-Atlantic Ridge rift valley: tectonics and volcanics. *Mar. Geophys. Res.*, 10:233–259.
- Edmond J.M., Campbell, A.C., Palmer, M.R., German, C.R., Klinkhammer, G.P., Edmonds, H.N., Elderfield, H., Thompson, G., and Rona, P., 1995. Time series studies of vent fluids from the TAG and MARK sites (1986, 1990): Mid-Atlantic Ridge: a new solution chemistry model and a mechanism for Cu/Zn zonation in massive sulfide ore bodies. In Parson, L.M., Walker, C.L., and Dixon, D.R. (Eds.), *Hydrothermal Vents and Processes*. Geol. Soc. Spec. Publ. London, 87:77–86.
- Edmond, J.M., Measures, C., McDuff, R.E., Chan, L.H., Collier, R., and Grant, B., 1979. Ridge crest hydrothermal activity and the balances of the major and minor elements in the ocean: the Galapagos data. *Earth Planet. Sci. Lett.*, 46:1–18.
- Franklin, J.M., Lyndon, J.W., and Sangster, D.F., 1981. Volcanic-associated massive sulfide deposits. *Econ. Geol.*, 75th Anniv. Vol., 75:485–627.
- Gal'chenko, V.F., Pimenov, N.V., Lein, A.Y., Galkin, S.V., Moskalev, L.I., and Ivanov, M.V., 1989. Autotrophic CO<sub>2</sub> assimilation in tissues of the shrimp *Rimicaris exoculata* from a hydrothermal region in the Mid-Atlantic Ridge. *Dokl. Akad. Nauk*, 308:1478–1481.
- Galkin, S.V., and Moskalev, L.I., 1990. Hydrothermal fauna of the Mid-Atlantic Ridge. *Okeanologia*, 30:842–847.
- Gillis, K.M., and Robinson, P.T., 1990. Patterns and processes of alteration in the lavas and dykes of the Troodos Ophiolite, Cyprus. *J. Geophys. Res.*, 95:21523–21548.
- Gillis, K.M., and Thompson, G., 1993. Metabasalts from the Mid-Atlantic Ridge: new insights into hydrothermal systems in slow-spreading crust. *Contrib. Mineral. Petrol.*, 113:502–523.
- Grassle, J.F., Humphris, S.E., Rona, P.A., Thompson, G., and Van Dover, C.L., 1986. Animals at Mid-Atlantic Ridge hydrothermal vents. *Eos*, 67:1022.
- Harper, G.D., Bowman, J.R., and Kuhns, R., 1988. A fluid, chemical, and stable isotope study of subseafloor metamorphism of the Josephine ophiolite, California-Oregon. *J. Geophys. Res.*, 93:4625–4656.
- Hart, S.R., and Staudigel, H., 1989. Isotopic characterization and identification of recycled components. In Hart, S.R., and Gülen, L. (Eds.), *Crust/Mantle Recycling at Convergence Zones*: Hingham, MA (Kluwer Acad.), 15–28.
- Herzig, P.M., Hannington, M.D., Scott, S.D., Maliotis, G., Rona, P.A., and Thompson, G., 1991. Gold-rich seafloor gossans in the Troodos ophiolite and on the Mid-Atlantic Ridge. *Econ. Geol.*, 86:1747–1755.
- Hoffman, A.W., and White, W.M., 1982. Mantle plumes from ancient oceanic crust. *Earth Planet. Sci. Lett.*, 57:421–436.
- Humphris, S.E., Kleinrock, M.C., and the Deep-TAG Team, 1994. Detailed morphology and the distribution of venting at the active TAG hydrothermal mound, 26°N, Mid-Atlantic Ridge. *Eos*, 75:660.
- Humphris, S.E., and Thompson, G., 1978. Hydrothermal alteration of basalts by seawater. *Geochim. Cosmochim. Acta*, 42:107–125.
- Ixer, R.A., Alabaster, T., and Pearce, J.A., 1984. Ore petrography and geochemistry of massive sulphide deposits within the Semail Ophiolite, Oman. *Trans. Min. Metall., Sect. B*, 93:B114–B124.
- Jacobson, R.S., 1992. Impact of crustal evolution on changes of the seismic properties of the uppermost oceanic crust. *Rev. Geophys.*, 30:23–42.
- Johnson, H.P., and Semyan, S.W., 1994. Age variation in the physical properties of oceanic basalts: implications for crustal formation and evolution. *J. Geophys. Res.*, 99:3123–3134.
- Karson, J.A., and Rona, P.A., 1990. Block tilting, transfer faults and structural control of magmatic and hydrothermal processes in the TAG area, Mid-Atlantic Ridge, 26°N. *Geol. Soc. Am. Bull.*, 102:1635–1645.
- Kleinrock, M.C., Humphris, S.E., and the Deep-TAG Team, 1994. The TAG region on the Mid-Atlantic Ridge: results from a recent near-bottom survey. *Eos*, 75:669.
- Kong, L.S.L., 1990. Variations in structure and tectonics along the Mid-Atlantic Ridge, 23°N and 26°N [Ph.D. dissert.]. MIT/WHOI Joint Program, Woods Hole, MA.
- Kong, L.S.L., Solomon, S.C., and Purdy, G.M., 1992. Microearthquake characteristics of a mid-ocean ridge along axis. *J. Geophys. Res.*, 97:1659–1685.
- Lalou, C., Bricquet, E., and Reyss, J.L., 1993a. Chronology of recently discovered hydrothermal mounds in the TAG area. *Eos*, 74:100.
- Lalou, C., Reyss, J.L., Bricquet, E., Arnold, M., Thompson, G., Fouquet, Y., and Rona, P.A., 1993b. New age data for Mid-Atlantic Ridge hydrothermal sites: TAG and Snakepit geochronology revisited. *J. Geophys. Res.*, 98:9705–9713.
- Lalou, C., Thompson, G., Arnold, M., Bricquet, E., Druffel, E., and Rona, P.A., 1990. Geochronology of TAG and Snake Pit hydrothermal fields, Mid-Atlantic Ridge: witness to a long and complex hydrothermal history. *Earth Planet. Sci. Lett.*, 97:113–128.
- Lin, J., Purdy, G.M., Schouten, H., Sempéré, J.-C., and Zervas, C., 1990. Evidence from gravity data for focused magmatic accretion along the Mid-Atlantic Ridge. *Nature*, 344:627–632.
- Lister, C.R.B., 1974. On the penetration of water into hot rock. *Geophys. J. R. Astron. Soc.*, 39:465–509.
- Lowell, R.P., Van Cappellen, P., and Germanovich, L.N., 1993. Silica precipitation in fractures and the evolution of permeability in hydrothermal upflow zones. *Science*, 260:192–194.
- Lowell, R.P., Rona, P.A., and Von Herzen, R.P., 1995. Seafloor hydrothermal system spreading centers. *J. Geophys. Res.*, 100:327–352.
- McGregor, B.A., Harrison, C.G.A., Lavelle, J.W., and Rona, P.A., 1977. Magnetic anomaly pattern on the Mid-Atlantic Ridge crest at 26°N. *J. Geophys. Res.*, 82:231–238.
- McGregor, B.A., and Rona, P.A., 1975. Crest of Mid-Atlantic Ridge at 26°N. *J. Geophys. Res.*, 80:3307–3314.
- Mével, C., 1987. Evolution of oceanic gabbros from DSDP Leg 82: influence of the fluid phase on metamorphic crystallization. *Earth Planet. Sci. Lett.*, 83:67–79.
- Nehlig, P., and Juteau, T., 1988. Deep crustal seawater penetration and circulation at ocean ridges: evidence from the Oman ophiolite. *Mar. Geol.*, 84:209–228.

- Purdy, G.M., Sempéré, J.-C., Schouten, H., et al., 1990. Bathymetry of the Mid-Atlantic Ridge, 24°–31°N: a map series. *Mar. Geophys. Res.*, 12:247–252.
- Reysenbach, A.-L., and Deming, J.W., 1991. Effects of hydrostatic pressure on growth of hyperthermophilic archaeobacteria from the Juan de Fuca Ridge. *Appl. Environ. Microbiol.*, 57:1271–1274.
- Rona, P.A., 1980. TAG hydrothermal field: Mid-Atlantic Ridge at latitude 26°N. *J. Geol. Soc. London*, 137:385–402.
- Rona, P.A., Bogdanov, Y.A., Gurvich, E.G., Rimski-Kursakov, A., Sagalevitch, A.M., Hannington, M.D., and Thompson, G., 1993a. Relict hydrothermal zones in the TAG hydrothermal field, Mid-Atlantic Ridge 26°N, 45°W. *J. Geophys. Res.*, 98:9715–9730.
- Rona, P.A., Hannington, M.D., Raman, C.V., Thompson, G., Tivey, M.K., Humphris, S.E., Lalou, C., and Petersen, S., 1993b. Active and relict seafloor hydrothermal mineralization at the TAG hydrothermal field, Mid-Atlantic Ridge. *Econ. Geol.*, 18:1987–2013.
- Rona, P.A., Klinkhammer, G., Nelsen, T.A., Trefry, J.A., and Elderfield, H., 1986. Black smokers, massive sulfides and vent biota at the Mid-Atlantic Ridge. *Nature*, 321:33–37.
- Rona, P.A., Petersen, S., Hannington, M.D., Becker, K., Von Herzen, R.P., Naka, J., Hertz, P.M., and Thompson, G., 1993c. Relict hydrothermal zones of TAG hydrothermal field, Mid-Atlantic Ridge, 26°N. *Eos*, 74:98.
- Rona, P.A., and Scott, S.D., 1993. A special issue on sea-floor hydrothermal mineralization: new perspectives. *Econ. Geol.*, 88:1935–1975.
- Rona, P.A., Thompson, G., Mottl, M.J., Karson, J.A., Jenkins, W.J., Graham, D., Mallette, M., Von Damm, K., and Edmond, J.M., 1984. Hydrothermal activity at the TAG hydrothermal field, Mid-Atlantic Ridge crest at 26°N. *J. Geophys. Res.*, 89:11365–11377.
- Rosenberg, N.D., Spera, F.J., and Haymon, R.M., 1993. The relationship between flow and permeability field in seafloor hydrothermal systems. *Earth Planet. Sci. Lett.*, 116:135–153.
- Saccoccia, P.J., Ding, K., Berndt, M.E., et al., 1994. Experimental and theoretical perspectives on crustal alteration at mid-ocean ridges. In Lentz, D. (Ed.), *Alteration and Alteration Processes Associated with Ore-Forming Systems*. Geol. Assoc. Canada, Short Course Notes, 11:403–431.
- Sclater, J.G., Jaupart, C., and Galson, D., 1980. The heat flow through oceanic and continental crust and the heat loss of the Earth. *Rev. Geophys. Space Phys.*, 18:269–311.
- Sempéré, J.-C., Purdy, G.M., and Schouten, H., 1990. Segmentation of the Mid-Atlantic Ridge between 24°N and 30°40'N. *Nature*, 344:427–431.
- Smith, D.K., and Cann, J.R., 1990. Hundreds of small volcanoes on the median valley floor of the Mid-Atlantic Ridge at 24°–30°N. *Nature*, 348:152–155.
- , 1992. The role of seamount volcanism in crustal construction at the Mid-Atlantic Ridge (24°–30°N). *J. Geophys. Res.*, 97:1645–1658.
- , 1993. Building the crust of the Mid-Atlantic Ridge. *Nature*, 365:707–715.
- Stein, C.A., and Stein, S., 1994. Constraints on hydrothermal heat flux through the oceanic lithosphere from global heat flow. *J. Geophys. Res.*, 99:3081–3095.
- Stern, C., and Elthon, D., 1979. Vertical variations in the effects of hydrothermal metamorphism in Chilean ophiolites: their implications for ocean floor metamorphism. *Tectonophysics*, 55:179–213.
- Strens, M.R., and Cann, J.R., 1986. A fracture-loop thermal balance model of black smoker circulation. *Tectonophysics*, 122:307–324.
- Temple, D.G., Scott, R.B., and Rona, P.A., 1979. Geology of a submarine hydrothermal field, Mid-Atlantic Ridge, 26°N latitude. *J. Geophys. Res.*, 84:7453–7466.
- Thompson, G., 1983. Basalt-seawater interaction. In Rona, P.A., Boström, K., Laubier, L., and Smith, K.L. (Eds.), *Hydrothermal Processes at Seafloor Spreading Centers*: New York (Plenum), 225–278.
- Thompson, G., Humphris, S.E., Schroeder, B., Sulanowska, M., and Rona, P.A., 1988. Active vents and massive sulfides at 26°N (TAG) and Snakepit (23°N) on the Mid-Atlantic Ridge. *Can. Mineral.*, 26:697–711.
- Thompson, G., Mottl, M.J., and Rona, P.A., 1985. Morphology, mineralogy and chemistry of hydrothermal deposits from the TAG area, 26°N Mid-Atlantic Ridge. *Chem Geol.*, 49:243–257.
- Tivey, M.A., Rona, P.A., and Schouten, H., 1993. Reduced crustal magnetization beneath the active sulfide mound, TAG hydrothermal field, Mid-Atlantic Ridge 26°N. *Earth Planet. Sci. Lett.*, 115:101–115.
- Tivey, M.A., Schouten, H., Sempéré, J.-C., and Wooldridge, A., 1989. Implications of the 3D structure of the TAG magnetic anomaly on the Mid-Atlantic Ridge. *Eos*, 70:455.
- Tivey, M.K., Humphris, S.E., Thompson, G., Hannington, M.D., and Rona, P.A., 1995. Deducing patterns of fluid flow and mixing within the TAG active hydrothermal mound using mineralogical and geochemical data. *J. Geophys. Res.*, 100:12527–12555.
- Van Dover, C.L., Fry, B., Grassle, J.F., Humphris, S.E., and Rona, P.A., 1988. Feeding biology of the shrimp *Rimicaris exoculata* at hydrothermal vents on the Mid-Atlantic Ridge. *Mar. Biol.*, 98:209–216.
- Wirsen, C.O., Jannasch, H.W., and Molyneux, S.J., 1993. Chemosynthetic microbial activity at Mid-Atlantic Ridge hydrothermal vent sites. *J. Geophys. Res.*, 98:9693–9703.
- Wooldridge, A.L., Harrison, C.G.A., Tivey, M.A., Rona, P.A., and Schouten, H., 1992. Magnetic modeling near selected areas of hydrothermal activity on the Mid-Atlantic and Gorda ridges. *J. Geophys. Res.*, 97:10911–10926.
- Zonenshain, L.P., Kuzmin, M.I., Lisitsin, A.P., Bogdanov, Y.A., and Baranov, B.V., 1989. Tectonics of the Mid-Atlantic rift valley between TAG and MARK areas (26–24°N): evidence for vertical tectonism. *Tectonophysics*, 159:1–23.

Ms 158IR-101